J|A|C|S
ARTICLES
Published on Web 09/29/2006

Two-Dimensional Ordered β-Sheet Lipopeptide Monolayers

Silvia Cavalli,[†] Jan-Willem Handgraaf,[†] Emily E. Tellers,[†] Daniela C. Popescu,[‡] Mark Overhand,[†] Kristian Kjaer,[§] Vladimir Vaiser,[||] Nico A. J. M. Sommerdijk,[‡] Hanna Rapaport,*[,||] and Alexander Kros*[,†]

Contribution from the Leiden Institute of Chemistry, Leiden University, P.O. Box 9502, 2300 RA Leiden, The Netherlands, Laboratory of Macromolecular and Organic Chemistry, Eindhoven University of Technology, P.O. Box 513, 5600 MB Eindhoven, The Netherlands, Niels Bohr Institute, University of Copenhagen, DK-2100 Copenhagen, Denmark, and Department of Biotechnology Engineering, Ben Gurion University of the Negev, P.O. Box 653, 84105, Beer-Sheva, Israel

Received August 16, 2006; E-mail: a.kros@chem.leidenuniv.nl; hannarap@bgu.ac.il.

Abstract: A series of amphiphilic lipopeptides, ALPs, consisting of an alternating hydrophilic and hydrophobic amino acid residue sequence coupled to a phospholipid tail, was designed to form supramolecular assemblies composed of β-sheet monolayers decorated by lipid tails at the air−water interface. A straightforward synthetic approach based on solid-phase synthesis, followed by an efficient purification protocol was used to prepare the lipid−peptide conjugates. Structural insight into the organization of monolayers was provided by surface pressure versus area isotherms, circular dichroism, Fourier transform infrared spectroscopy, and Brewster angle microscopy. In situ grazing-incidence X-ray diffraction (GIXD) revealed that lipopeptides six to eight amino acids in length form a new type of 2D self-organized monolayers that exhibit β-sheet ribbons segregated by lipid tails. The conclusions drawn from the experimental findings were supported by a representative model based on molecular dynamics simulations of amphiphilic lipopeptides at the vacuum−water interface.

Introduction

The search for advanced materials and new fabrication strategies has become one of the essential aims of materials scientists. Progress in the design and characterization of "smart" nanostructures with predictable properties and functions enhances our understanding of molecular assembly and contributes to successful engineering of new supramolecular architectures.[1] Peptide motifs are particularly attractive as building blocks for generating highly defined self-assembled structures in a bottom-up approach. Their secondary structural elements are determined by a combination of hydrophobic, electrostatic, and hydrogen-bonding interactions.[22] Amphiphilic oligopeptide sequences and peptides modified with one or more alkyl tails have been shown to form various supramolecular organizations exhibiting α-helices,[3] antiparallel[4] or parallel β-sheet,[5] β-hairpins,[6] ribbons,[7] twisted ribbons,[8] and fibers.[9] Careful molecular designs allow control over the peptide conformation and intermolecular interactions thus providing specific types of nanometer-scale assembled scaffolds relevant for a broad range of applications.[10] Furthermore, amphiphilic oligopeptides and proteins have been used to generate well-ordered molecular assemblies at interfaces.[4,11] Planar peptide scaffolds, in the form of monolayers have been shown to template nucleation of inorganic crystals.[12,13]

[†] Leiden University.
[‡] Eindhoven University of Technology.
[§] University of Copenhagen.
[||] Ben Gurion University of the Negev.

(1) (a) Elemans J. A. A. W.; Rowan A. E.; Nolte, R. J. M. *J. Mater. Chem.* **2003**, *13*, 2661−2670. (b) Gao, X.; Matsui, H. *Adv. Mater.* **2005**, *17*, 2037−2050. (c) Lehn, J.-M. *Science* **2002**, *295*, 2400−2403.
(2) (a) Chen, P. *Colloids Surf., A* **2005**, *261*, 3−24. (b) Zhao, X.; Zhang, S. *Trends Biotechnol.* **2004**, *22*, 470−476. (c) Rajagopal, K.; Schneider, J. P. *Curr. Opin. Struct. Biol.* 2004, *14*, 480−486.
(3) Yu, Y.-C.; Berndt, P.; Tirrell, M.; Fields, G. B. *J. Am. Chem. Soc.* **1996**, *118*, 12515−12520.
(4) Rapaport, H.; Kjaer, K.; Jensen, T. R.; Leiserowitz, L.; Tirrell, D. A. *J. Am. Chem. Soc.* **2000**, *122*, 12523−12529.
(5) Sneer, R.; Weygand, M. J.; Kjaer, K.; Tirrell, D. A.; Rapaport, H. *ChemPhysChem* **2004**, *5*, 747−750.
(6) (a) Lowik, D. W. P. M.; Garcia-Hartjes, J.; Meijer, J. T.; van Hest, J. C. M. *Langmuir* **2005**, *21*, 524−526. (b) Rapaport, H.; Moller, G.; Knobler, C. M.; Jensen, T. R.; Kjaer, K.; Leiserowitz, L.; Tirrell, D. A. *J. Am. Chem. Soc.* **2002**, *124*, 9342−9343. (c) Schneider, J. P.; Pochan, D. J.; Ozbas, B.; Rajagopal, K.; Pakstis, L.; Kretsinger, J. *J. Am. Chem. Soc.* **2002**, *124*, 15030−15037.
(7) (a) Matsumura, S.; Uemura, S.; Mihara, H. *Chem.—Eur. J.* **2004**, *10*, 2789. (b) Aggeli, A.; Bell, M.; Carrick, L. M.; Fishwick, C. W. G.; Harding, R.; Mawer, P. J.; Radford, S. E.; Strong, A. E.; Boden, N. *J. Am. Chem. Soc.* **2003**, *125*, 9619−9628. (c) Aggeli, A.; Nyrkova, I. A.; Bell, M.; Harding, R.; Carrick, L.; McLeish, T. C. B.; Semenov, A. N.; Boden, N. *Proc. Natl. Acad. Sci. U.S.A.* **2001**, *98*, 11857−11862.
(8) (a) Marini, D. M.; Hwang, W.; Lauffenburger, D. A.; Zhang, S. G.; Kamm, R. D. *Nano Lett.* **2002**, *2*, 295. (b) Vauthey, S.; Santoso, S.; Gong, H. Y.; Watson, N.; Zhang, S. G. *Proc. Natl. Acad. Sci. U.S.A.* **2002**, *99*, 5355.
(9) (a) Behanna, H. A.; Donners, J. J. J. M.; Gordon, A. C.; Stupp, S. I. *J. Am. Chem. Soc.* **2005**, *127*, 1193−1200. (b) Li, L.-S.; Stupp, S. I. *Angew. Chem., Int. Ed.* **2005**, *44*, 1833−1836.
(10) Smeenk, J. M.; Otten, M. B. J.; Thies, J.; Tirrell, D. A.; Stunnenberg, H. G.; van Hest, J. C. M. *Angew. Chem. Int. Ed.* **2005**, *44*, 1968−1971.
(11) (a) Guofeng, X.; Weixun, W.; Groves, J. T.; Hecht, M. H. *Proc. Natl. Acad. Sci. U.S.A.* **2001**, *98*, 7, 3652−3657. (b) Kuzmenko, I.; Rapaport, H.; Kjaer, K.; Als-Nielsen, J.; Weissbuch, I.; Lahav, M.; Leiserowitz, L. *Chem. Rev.* **2001**, *101*, 1659−1696.
(12) Bekele, H.; Fendler, J. H.; Kelly, J. W. *J. Am. Chem. Soc.* **1999**, *121*, 7266−7267.
(13) Cavalli, S.; Popescu, D. C.; Tellers, E. E.; Vos, M. R. J.; Pichon, B. P.; Overhand, M.; Rapaport, H.; Sommerdijk, N. A. J. M.; Kros, A. *Angew. Chem., Int. Ed.* **2006**, *45*, 739−744.

Chart 1

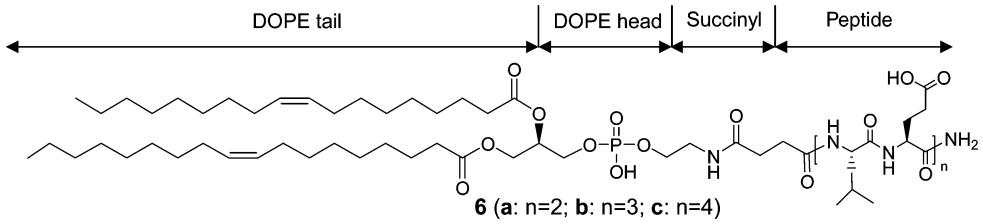

The lipopeptides discussed hereafter represent a first example of highly ordered peptide-based amphiphilic monolayers with a unique hybrid character. On the one hand the lipopeptides may organize into a well-defined architecture, conferred by the β-sheet folded peptide and on the other hand they exhibit the structurally flexible mono-unsaturated lipid tails. The conjugated phospholipid tail was introduced in order to increase the hydrophobicity of the molecular system, thus enhancing the tendency of the system to reside at the air−water interface. In a recent study of calcite crystallization on lipopeptide monolayers we demonstrated that structural adaptability plays a key role in the formation of a new type of indented, {10.0}-oriented, calcite crystals.[13]

This report describes an accurate molecular design strategy combined with a straightforward synthetic approach and in-depth structural characterization of lipopeptides using Langmuir monolayer experiments, Brewster angle microscopy real-time observations, and grazing-incidence X-ray diffraction measurements performed at the air−water interface.

Results and Discussion

Lipopeptide Design. The amphiphilic lipopeptides, ALPs, studied here (Chart 1), are composed of amphiphilic oligopeptide moieties (**6a**−**c**) with alternating hydrophobic and hydrophilic amino acid residues, $(Leu\text{-}Glu)_n$ interlinked by a succinyl moiety to the phospholipid tails, 1,2-dioleoyl-*sn*-glycero-3-phosphoethanolamine (DOPE). The sequential order of hydrophobic and hydrophilic amino acids induces the generation of β-sheet secondary structure at the air−water interface.[4] The peptide backbones in the β-sheet conformation are expected to lay with their long molecular axes parallel to the interface so that the hydrophobic side groups point toward the air and the hydrophilic side chains are distributed regularly on the water interface. Yet, with the hybrid nature of the ALPs we considered the possibility that the phospholipid tails would interfere with the β-sheet organization. We therefore sought the proper length of the peptide domain necessary to generate the β-sheet organization.[14] Three ALPs were synthesized, each exhibiting a different length of the peptidic part, $(Leu\text{-}Glu)_2$-, $(Leu\text{-}Glu)_3$-, and $(Leu\text{-}Glu)_4$, termed tetra-, hexa-, and octa-ALP, respectively (cf. **6a**, **6b**, and **6c** in Scheme 1).

Lipopeptide Synthesis. The synthetic approach toward ALPs with variable length of the peptidic part commenced with the synthesis of immobilized peptides **4a**−**c** using a standard Fmoc solid-phase peptide protocol (Scheme 1).[15] After removal of the Fmoc group the 1,2-dioleoyl-*sn*-glycero-3-phosphoethanolamine-*N*-succinic acid **2** was coupled to the anchored peptides.

Scheme 1. Synthesis of ALPs, **6a**−**c**[a]

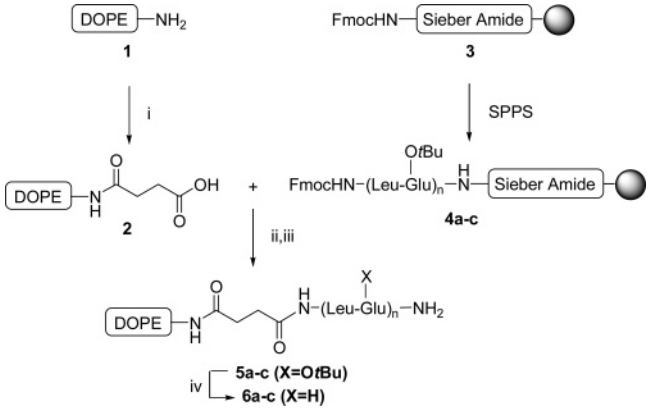

[a] (i) Succinic anhydride, TEA in DCM. Solid phase peptide synthesis (SPPS): (a) (Fmoc removal) 20% piperidine in NMP; (b) (coupling) PyBOP, Fmoc-Glu(O^{t}Bu)-OH or Fmoc-Leu-OH, DiPEA in NMP; (c) (capping) 5% Ac_2O, 5% 2,6-lutidine in NMP; iterated n times ($n = 2$, **4a**; $n = 3$, **4b**; $n = 4$, **4c**). (ii) (a) (Fmoc removal) 20% piperidine in NMP; (b) (coupling) PyBOP, DiPEA in DCM. (iii) Cleavage from the resin: 1% TFA in DCM. (iv) *t*-Bu removal: 90% TFA in H_2O.

The acid-labile Sieber amide resin permitted selective cleavage of the fully protected lipopeptides **5a**−**c** from the solid support under mild conditions (99/1 v/v dichloromethane/trifluoroacetic acid),[16] followed by smooth purification using silica gel flash chromatography and RP-HPLC. *t*-Butyl protecting groups were subsequently removed under acidic conditions (90/10 v/v trifluoroacetic acid/water) yielding the target ALPs (**6a**−**c**) that were purified by RP-HPLC and characterized by LC/ESI-MS and NMR spectroscopy. The purified ALPs were obtained in overall yield ranging from 35 to 55%.

Surface Pressure−Molecular Area (π-*A*) Isotherms. Surface pressure versus molecular area (π-*A*) isotherms of DOPE **1** and the ALPs (**6a**−**c**) on deionized water are shown in Figure 1. In all cases stable monolayers were obtained, which collapsed upon compression at a surface pressure between 40 and 50 mN/m. The isotherm of DOPE is characterized by a lift-off pressure at ∼90 Å^2/molecule that is attributed to liquid and condensed phases typical of phospholipids with cis unsaturated tails.[17] The area per molecule indicated by a tangent line drawn to the steepest part in the surface pressure curve provides a measure of the limiting area per molecule (Figure 1). The DOPE isotherm indicates an area per molecule of 71 Å^2/molecule. In an antiparallel β-sheet arrangement, a residue contributes ∼3.4 Å to the projected length of the peptide while the distance between adjacent β-strands along the hydrogen bond direction is ∼4.7 to 4.8 Å. With these dimensions the peptidic part of tetra-ALP (**6a**) should occupy an area of ca. 4 × 3.4 Å ×

(14) Aggelli, A.; Bell, M.; Boden, N.; Keen, J. N.; McLeish, T. C. B.; Nyrkova, I.; Radford, S. E.; Semenov, A. *J. Mater. Chem.* **1997**, *7*, 1135−1145.
(15) (a) Chan, W. C.; White, P. D. *Fmoc Solid-phase Peptide Synthesis: A Practical Approach*; Oxford University Press: Oxford, 2000. (b) Fields, G. B.; Noble, R. L *Int. J. Pept. Protein Res.* **1990**, *35*, 161−214.
(16) Sieber, P. *Tetrahedron Lett.* **1987**, *28*, 2107−2110.
(17) Shah, D. O. *Monolayers of Lipids in Relation to Membranes*; Pergamon Press: Oxford, 1972.

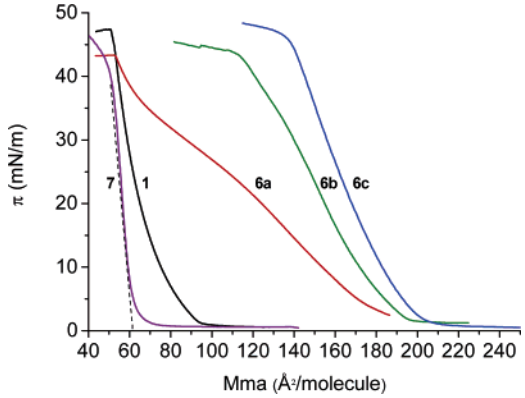

Figure 1. Surface pressure−area (π−A) isotherms of DOPE **1** (black line), tetra-ALP **6a** (red line), hexa-ALP **6b** (green line), octa-ALP **6c** (blue line), and Ac-(Leu-Glu)$_4$-NH$_2$ **7** (purple line) on deionized water subphase (pH 5.3) measured at 20 °C. The limiting molecular areas were calculated by extrapolating the slope of each curve in the steepest part to zero pressure (see dashed line as an example for **7**). Films were allowed to equilibrate for 10 min before compression.

4.8 Å ∼65 Å^2/molecule.[4,11a] The isotherm of tetra-ALP, displays a lift-off pressure at ∼192 Å^2/molecule that is larger than the sum of the estimated area of the peptidic part (65 Å^2) and the lift-off area, 90 Å^2 per DOPE molecule, extracted from the phospholipid isotherm (Figure 1). It is reasonable to attribute the trajectory of the tetra-ALP isotherm to expanded and condensed liquid phases. These phases are followed by film collapse at approximately the same limiting area per molecule as DOPE, implying that in the fully compressed state the peptidic part of tetra-ALP immerses within the subphase and the lipid tails are packed similarly as in the DOPE compressed film. This behavior indicates that the peptide is too short to organize into β-sheets at the air−water interface. In summary, the tetra-ALP isotherm implies that the peptide part of ALP starts off residing at the air−water interface and upon compression it submerges into the subphase. This structural flexibility is reflected in the CD and FTIR measurements described later. Noteworthy, it has been suggested that a peptide must have a minimum of six residues to form stable β-sheet structures.[14] Extension of the peptide domain from four to six and eight residues resulted in more ordered assembled structures. Hexa-ALP (**6b**) exhibits a lift-off pressure at ∼195 Å^2/molecule that is in good agreement with the estimated contribution of both the peptidic part in β-sheet conformation, 6 × 4.8 Å × 3.4 Å ∼98 Å^2 and the lipidic part (90 Å^2/molecule). A steady increase in surface pressure leads to the film collapse at ∼110 Å^2/molecule, corresponding to the peptidic part of hexa-ALP. Similar isotherm characteristics are obtained for octa-ALP with a lift-off pressure at ∼205 Å^2/molecule that is somewhat smaller than the sum of the peptidic and lipid contributions, ∼220 Å^2 (i.e., 8 × 4.8 Å × 3.4 Å = ∼130 Å^2 plus 90 Å^2). The octa-ALP film collapses at ∼135 Å^2/molecule that matches well the area of the peptidic part in the β-sheet conformation. Both the hexa-ALP (**6b**) and octa-ALP (**6c**) isotherms suggest that the β-sheet assemblies resist film compression up to the film collapse and that the lipid part does not reside at the air−water interface in the compressed state.

Circular Dichroism (CD) and Attenuated Total Reflectance Fourier Transform Infrared (ATR-FTIR). Information about secondary structures of the peptide domains was obtained by transferring the compressed lipopeptide monolayers onto different solid supports, which were analyzed using spectroscopic techniques, CD, and ATR-FTIR. For CD studies a hydrophilic quartz plate was used, while for the ATR-FTIR spectra a hydrophobic surface (ZnSe) was employed (see Supporting Information). Indeed, similar results were obtained from the two different spectroscopic methods, suggesting that the nature of the substrate did not alter the assembly arrangement. Furthermore the CD and FTIR studies supported the outcomes deduced from the Langmuir experiments. The tetra-ALP monolayer transferred poorly onto the quartz plates, compared to the other ALPs, possibly because of the relatively weak intermolecular interactions and low degree of order that characterizes its assemblies. Consequently, the CD measurements of tetra-ALP exhibited weak and noisy absorption spectra that did not allow a definite interpretation of the data. By contrast, hexa- and octa-ALP monolayers were successfully transferred (transfer ratio close to 1) onto quartz plates. The CD spectrum of hexa-ALP displayed a minimum at 219 nm and a maximum at 201 nm (Figure 2) and was attributed to β-sheet assemblies.[18] In the CD spectrum of octa-ALP the signal-to-noise ratio improved markedly. A sharp signal characterized by a maximum at 202 nm and a minimum at 218 nm was observed, indicating again a well-defined β-pleated sheet organization. In addition, CD spectra of multilayers of compound octa-ALP (**6c**) were also measured. Samples were obtained by covering the quartz plate surface with a solution of **6c** in 10/90 (v/v) TFA/chloroform (same solution used for the Langmuir experiments), and the solvent was allowed to dry in air at room temperature. The CD spectrum (see Supporting Information) displayed two minima, one at 219 and the other at 208 nm, and a maximum at 193 nm indicative of a α-helical conformation.[19] Thus, it appears that the assembly of the monolayer at the air−water interface induces the β-sheet conformation.

The ATR-FTIR spectrum of tetra-ALP displayed a strong and broad amide I band at 1657 cm^{-1}, a weaker amide II band at 1536 cm^{-1} and an amide A band at 3280 cm^{-1} (Table 1). These wavenumbers appear indicative of an α-helix arrangement. By contrast, the monolayers of hexa- and octa-ALP displayed absorption bands indicative of β-sheet structures, confirming the CD observations. The spectrum of hexa-ALP monolayer was characterized by an amide I band at 1630 cm^{-1} and an additional band at 1694 cm^{-1} which indicates that the β-sheet formation adopts the antiparallel organization (Figure 2a,c).[20] Amide II and A were found at 1536 and 3278 cm^{-1}, respectively (Table 1). Octa-ALP displayed a strong and sharp band at 1628 and at 1694 cm^{-1} confirming the β-sheet antiparallel order (Figure 2b,d). Multilayers of octa-ALP, that were prepared by drop casting from a 10/90 (v/v) TFA/chloroform solution, were also studied by FTIR spectroscopy. An amide I band at ∼1650 cm^{-1} was found, which may be attributed to α-helical conformation. Once again, this result indicates that the β-sheet organization is achieved during the assembly of the ALPs monolayer at interfaces.

To study the effect of the lipid tail on the peptide domain assembly, the N-acetylated and C-amidated octapeptide Ac-

(18) Rodger, A.; Nordén, B. *Circular Dichroism and Linear Dichroism*; Oxford University Press: New York, 1997, p 21.
(19) This is typical for α-helices. The folding into α-helix was probably induced by the presence of the halogenated solvent.
(20) (a) Bandekar, J. *Biochim. Biophys. Acta* **1992**, *1120*, 123−143. (b) Jackson, M.; Mantsch, H. H. *Crit. Rev. Biochem. Mol. Biol.* **1995**, *30*, 95−120.

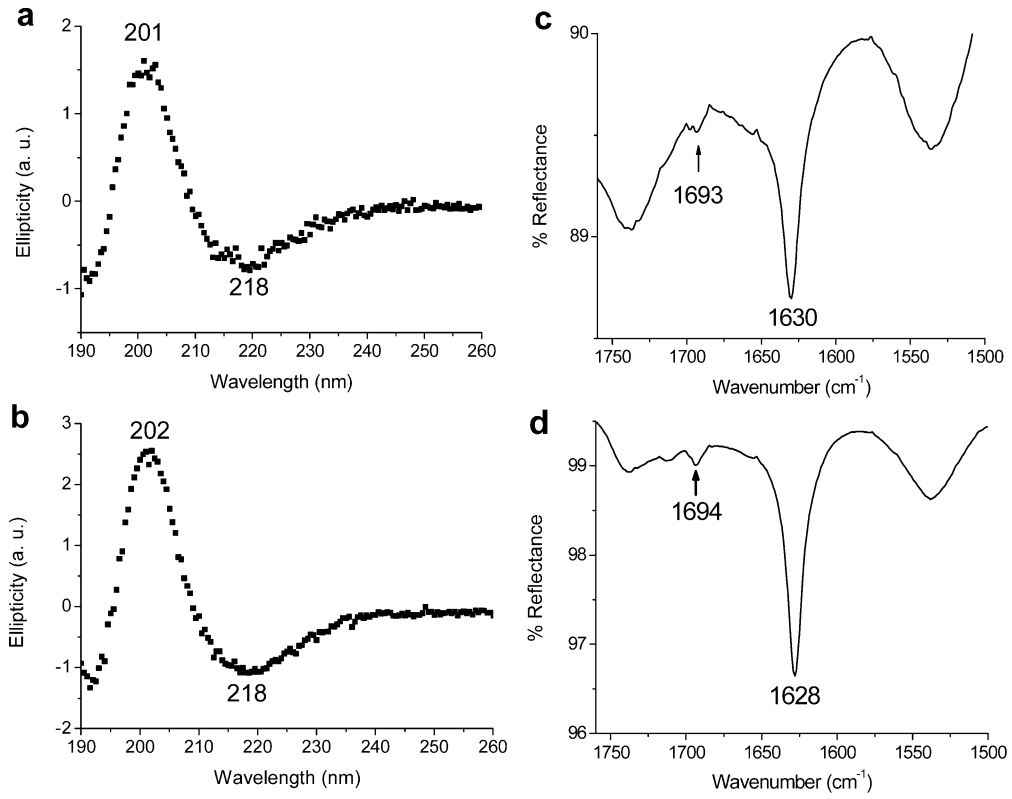

Figure 2. CD spectra of monolayers (a) **6b** and (b) **6c**; FT-IR spectra of monolayers (c) **6b** and (d) **6c**. The monolayers were transferred onto a hydrophilic quartz plate for CD and a hydrophobic ZnSe crystal for ATR FT-IR analysis by upstroke vertical deposition at a constant surface pressure (π) of 15, 20, and 30 mN/m for **6a**, **6b**, and **6c**, respectively.

Table 1. Amide A, I and II Values Found for Monolayers of **6a**−**c** Transferred onto ATR ZnSe Crystal

	amide A cm^{-1}	amide I cm^{-1}	amide II cm^{-1}
6a	3280	1657	1536
6b	3278	1693	1536
		1630	
6c	3275	1694	1538
		1628	

$(Leu\text{-}Glu)_4\text{-}NH_2$ (**7**) was also prepared and investigated at the air−water interface. The octa-peptide monolayer appeared to organize in a β-sheet fashion at the interface. However, since the peptide limiting area per molecule was found to be smaller than the estimated value, on the basis of the known dimensions of β-sheets (61 vs 130 $Å^2$/molecule), it is reasonable to assume that the eight residue peptide partially dissolved in the water subphase. In addition, the octapeptide monolayer exhibits a steeper increase in the surface pressure area isotherm compared to that of octa-ALP, pointing to the higher compressibility of the lipopeptide that is conferred by the addition of the unsaturated lipid. (Figure 1).

Brewster Angle Microscopy (BAM). Figure 3 shows BAM images of the octa-ALP monolayer along film compression from 0.20 to ∼44 mN/m. Figure 3a (π = 0.20 mN/m) shows the film immediately after the evaporation of the solvent. Strikingly, compact domains, almost covering the water surface, could already be observed at this low surface pressure, pointing to the self-assembling tendency of octa-ALP. Upon increase in surface pressure these domains fused to form a continuous film (Figure 3b,c; π = 0.30 and π = 23 mN/m, respectively).

In Situ Grazing-Incidence X-ray Diffraction (GIXD) Measurements. GIXD measurements were performed to elucidate the two-dimensional structure of the lipopeptide monolayers at the air−water interface. Tetra-ALP with its short four-residue peptide did not exhibit any Bragg peak, indicating no measurable formation of ordered assemblies. The monolayer of hexa-ALP, at surface pressure π = 0.5 mN/m, yielded two Bragg peaks. One Bragg peak at q_{xy} = 1.3055 $Å^{-1}$, corresponding to 4.81 Å spacing and the second at q_{xy} = 0.1209 $Å^{-1}$, corresponding to 52 Å spacing (Table 2). The ∼4.75 to 4.8 Å spacing is typical of β-pleated peptide strands interlinked by N−H···O═C interstrand hydrogen bonds which constitutes strong evidence for the formation of a β-sheet assembly at the air−water interface. However, this Bragg peak was weak, indicating a limited detectable order along the interstrand hydrogen bonded direction (Figure 4, along *a*). The estimated length of the six residues peptidic part in β-strand conformation (with free amine and carboxy termini) is ∼3.45 × 6 = ∼21 Å. The linker at the N-terminus of the peptide that is composed of a succinyl group attached to the hydrophilic headgroup of the phospholipid (Chart 1), in an extended conformation, may reach ∼14 Å. We hypothesize that the lipid tails avoid contact with the water interfaces and thus fold back onto the peptide to interact with the β-strand Leu hydrophobic side chains. Since the detected 52 Å spacing is appreciably longer than the length of the peptidic and the linker parts, 35 Å, we propose a model that exhibits a spacing generated by two lipopeptides along *b* (Figure 4). The assembly in Figure 4 depicts the peptidic part of the ALPs arranged in the antiparallel mode along the *a* direction, as indicated by the FTIR measurements discussed above. The ALPs along the *b* direction are related in general

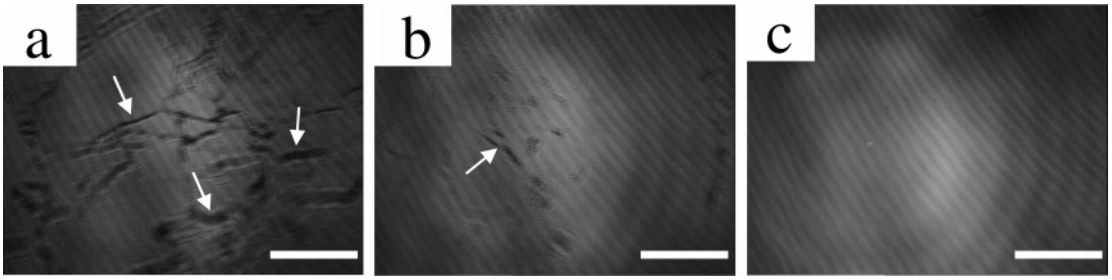

Figure 3. BAM images of the monolayer of **6c** taken at different surface pressure (π) and area (A): (a) $\pi = 0.20$ mN/m, $A = 277$ Å^2/molecules; (b) $\pi = 0.30$ mN/m, $A = 245$ Å^2/molecules; (c) $\pi = 22.81$ mN/m, $A = 180$ Å^2/molecules. Scale bar = 100 μm. Arrows mark crack lines in the octa-ALP monolayer.

Table 2. GIXD Data of Hexa-ALP (**6b**) and Octa-ALP (**6c**)

	(0,1)[f]						(2,0)[e]			
π mN/m	q_{xy} Å^{-1}	d[a] Å	L_{xy}[b] Å	I_{max}[c] a.u.	q_z[d] Å^{-1}	h_z[d] Å	q_{xy} Å^{-1}	d Å	L_{xy} Å	I_{max} a.u.
				Hexa-ALP (**6b**)						
0.5	0.1209	52.0	520	5994	0.369	16.2	1.3055	4.81	47	1711
10	0.1379	45.6	553	12936	0.375	17.9	1.3149	4.78	60	2490
10	0.1373	45.8	577	8802	0.382	16.6	1.3128	4.79	46	2033
				Octa-ALP (**6c**)						
0.7	0.0990	63.5	487	2398	0.293	17.7	1.3050	4.81	52	1900
0.5[g]	0.1070	58.7	365	5429	0.333	16.2	1.3147	4.78	40	4243
1.1	0.1013	62.0	478	4917	0.286	15.7	1.3095	4.80	40	4090
13.1	0.1327	47.3	373	13433	0.369	17.1	1.3149	4.78	48	6624
19.9	0.1369	45.9	416	12301	0.382	17.5	1.3180	4.77	48	6493
30.1	0.1602	39.2	329	9248	0.370	26.0	1.3225	4.75	48	6408
30.1	0.1595	39.4	280	8302	0.369	29.6	1.3225	4.75	51	4095

[a] The spacing corresponding to q_{xy}, $d = 2\pi/q_{xy}$. [b] The coherence length of the ordered domain along the spacing direction, $L_{xy} = 0.9 \times 2\pi/\text{fwhm}_{xy}$ where the fwhm_{xy} is the full width at half-maximum of the Bragg peak at q_{xy}. [c] The maximum intensity of the Bragg peak. [d] Values q_z and h_z are the Bragg rod position maxima and height, respectively. The height is estimated according to $h_z = 0.9 \times 2\pi/\text{fwhm}_z$ where the fwhm_z is that of the Bragg rod. The full $I(q_z)$ patterns of the Bragg rod data are provided in Figures 5a and S3. [e] The q_z and h_z values of the (2,0) were not extracted because of the relatively low intensity of these Bragg rods. [f] The compressibility of the crystalline lattice along (0,1) is estimated with the equation $C_c = d \ln d_{(0,1)}/d\pi$; for hexa-ALP, based on the first two data points in the table, $C_c = [(\ln 45.6 - \ln 52.0)/(10 - 0.5)] \times [1000 \text{ mN/1N}] = 13.8$ m/N. The compressibility of octa-ALP, 12 m/N, was evaluated based on a linear fit to $\ln d_{(0.1)}$ vs π, where the compressibility equals the slope of this line (Figure S4 Supporting Information). [g] This data point is unusual as it shows an increase in surface pressure with an increase in $d(0,1)$. This behavior is attributed to film relaxation.

by 2-fold or pseudo-2-fold symmetry, to account for a spacing that is longer than the length of the peptide and linker. The symmetry along *b* could be driven by preferable hydrogen bonds between the C-amide termini which have been detected in a previously reported system of amphiphilic β-sheet peptides.[5] We hypothesize that the repeat structural motif in the ordered assembly is composed of four ALPs, where the C-amide to C-amide oriented peptides along the *b* direction, ALP monomers attach along the *a* direction in the antiparallel mode, with the linker phosphates hydrogen-bonded to the amides. These assemblies grow along the *a* direction to form double-ALP width ribbons. The amide−phosphate or amide−amide interactions at the rim of the ribbon cannot be formed as in the center of the ribbon (Figure 4) owing to plausible distortions in the β-strands or mismatches in amide−phosphate interactions at the rim of the double ALP width ribbons (along the *b* direction). The absence of a (0,2) Bragg reflection may also point to disorder along the *b* direction.

According to the estimated dimensions described above, the hexa-ALP (0,1) spacing may extend to $35 \times 2 = 70$ Å. However, the detected Bragg peak indicated only $d(0,1) = 52$ Å. Various factors and combinations thereof may explain the discrepancy between the estimation of the ribbon maximum width and the observed spacing. It is possible that the flexible linker with the phosphate in its end, folds to contribute less than the 14 Å to the repeat distance. The assembly could be characterized by a unit cell with an angle $\gamma \neq 90°$ (between *a* and *b* axes, see Figure 4 legend) that would result in a spacing shorter than the estimated length of two ALPs.[5] In addition, the β-sheet backbones may also be slightly bent out of, or within, the plane of the air−water interface because of interactions of the hydrophobic side chains with the lipid tails. Bent strands would also contribute to an edge-to-edge ribbon distance smaller than that estimated above.

The full widths at half-maxima, fwhm (q_z), of the hexa-ALP Bragg rods along q_z indicate a crystalline film ~16.2 to 17.9 Å thick (Table 2). As a thickness of ~9 Å[6b] has been found for peptide β-sheet monolayers, this result supports the hypothesis that the lipid tails fold back onto the peptide and contribute ~7 to 9 Å to the film thickness. The crystalline coherence length L_{xy}, a measure of the extent of lateral molecular order, estimated from the fwhm (q_{xy}) of the Bragg peaks, is approximately 520−580 Å along the (0,1) direction and ~46 to 60 Å along the (2,0). The compression of the hexa-ALP monolayer to $\pi = 10$ mN/m resulted in a shift of the Bragg peak position to a higher q_{xy} value, 0.1379 Å^{-1} corresponding to $d = 45.6$ Å, indicating that the hexa-ALP crystalline structure exhibits a measurable compressibility.[21] A compressibility of 13.8 m/N has been estimated for hexa-ALP on the basis of the first two diffraction data points (see Table 2 legend) measured along the isotherm. The (0,1) Bragg rod patterns, $I(q_z)$ (Table 2, Figures 5a and S3), overall, did not change in shape, suggesting that on compression there is no appreciable change in the electron density profile of the ordered film along the *z* direction (normal to the air−water interface). This is in contrast to our recent studies on compression of P_{Glu}-5 which exhibited significant changes in Bragg rod patterns upon compression[21] attributed to bending of the β-strands out of the air−water interface. As shall be described later, the Bragg rods data of octa-ALP under compression indicated a behavior similar to that of P_{Glu}-5. The fact that under compression hexa-ALP exhibits almost no change in the overall shape of the (0,1) Bragg rod patterns suggests that most of the conformational changes occur in the lattice *xy* plane by bending, for example, the backbone axes in the *xy* plane, thus shortening the dimer edge-to-edge length along the *b* direction. Further compression of the collapsed hexa-ALP film (Table 2, the third measured point along the isotherm at $\pi = 10$ mN/m), did not alter the (0,1) Bragg peak position, indicating

(21) Isenberg, H.; Kjaer, K.; Rapapport, H. *J. Am. Chem. Soc.* **2006**, *128*, 12468−12472.

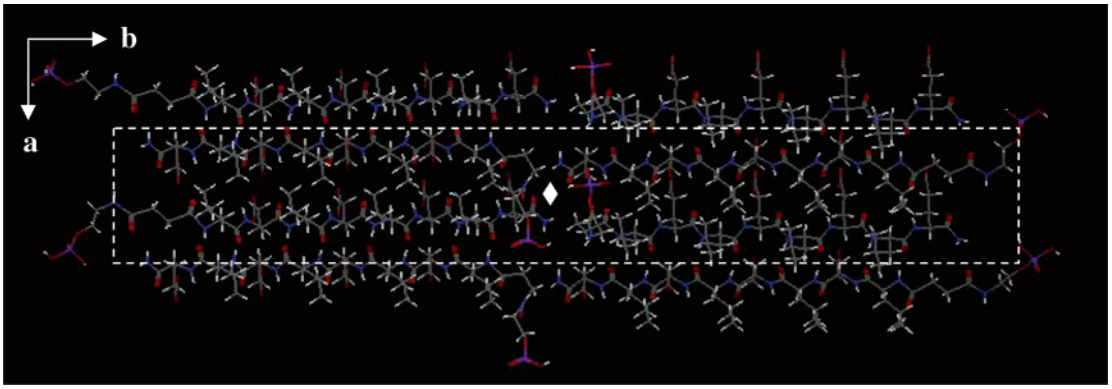

Figure 4. Proposed packing model for hexa- and octa-ALP molecules demonstrating the main structural elements that may lead to the appearance of an (0,1) Bragg peak.

that at this state, the ordered film resists the compression and the disordered part of the film yields, probably by buckling into nonordered multilayered film.

An octa-ALP monolayer on water exhibited a (0,1) and a (2,0) Bragg peak at $q_{xy} = 0.0990$ and 1.3050 Å^{-1}, respectively (Table 2), in a proposed assembly similar to that shown in Figure 4. The estimated length of the eight residues β-strand of octa-ALP is $\sim 3.45 \times 8 = \sim 28$ and 42 Å, with the addition of the linker length, in stretched conformation ($\sim$14 Å) at the N-terminus (Chart 1). Similar to the hexa-ALP case discussed above, the detected 62 Å spacing is appreciably longer than the estimated length of the peptidic and the linker parts (42 Å). We therefore propose that the octa-ALP monolayer packs into a lattice with structural characteristics similar to those of the hexa-ALP, with two neighboring octa-ALPs in a unit cell that may extend to $42 \times 2 = 84$ Å repeat distance, along *b* (Figure 4). The discrepancy between the detected (0,1) spacing and the estimated length (along the *b* direction) of two neighboring peptides may be explained by the same scenarios mentioned above for hexa-ALP. The (0,1) Bragg peak was found to shift to higher q_{xy} values upon compression, showing a reduction of $\sim$24 Å in the detected spacing with an increase to 30 mN/m in surface pressure (Table 2 and Figure 5C). The diffraction measurements of octa-ALP (Table 2) suggest that up to $\pi \approx 1$ mN/m the film is highly compressible, whereas at higher surface pressure values a compressibility of 12 m/N maybe evaluated on the basis of the measured diffraction data (Table 2 and Figure S4, Supporting Information). Unlike hexa-ALP, on compression to high π-values, the general shape of the (0,1) Bragg rod of octa-ALP showed a shift in the q_z maximum to higher values (Table 2) that indicates significant change in electron density along the direction normal to the air−water interface. Similar changes in Bragg rod patterns along film compression were recently reported in P_{Glu}-5 and attributed to β-strands elastic bending. It is likely also that octa-ALP ordered assemblies behave similarly to P_{Glu}-5 and bend their peptidic backbone out of the water interface. The (0,1) Bragg rods obtained at $\pi =$ 1.1, 13.1, and 19.9 mN/m (Table 2 and Figure 5C) indicate a crystalline film $\sim$15.7 to 17.5 Å thick. A significant increase in film thickness to $\sim$26 to 39.6 Å was observed for the collapsing film at 30.1 mN/m (Figure 5). This increase in the estimated thickness of the ordered film and the significant change in the Bragg rod pattern at $\pi = 30.1$ mN/m (i.e., the appearance of a new modulation at low q_z, Figure 5C) may be attributed to the formation of an ordered multilayer structure.

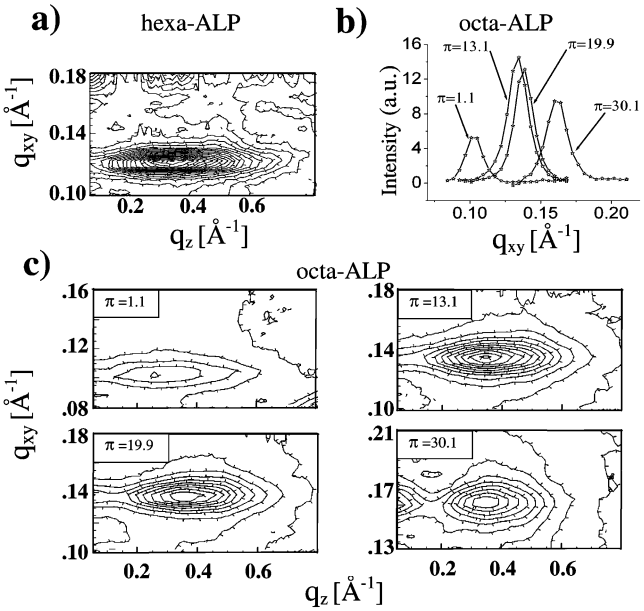

Figure 5. (a) GIXD contour plot of hexa-ALP (**6b**) for $\pi = 0$; (b) measured GIXD Bragg peaks of octa-ALP (**6c**); (c) GIXD contour plots of octa-ALP (**6c**) obtained at $\pi = 1.1$, 13.1, 19.9, and 30.1 mN/m.

Molecular Dynamic (MD) Simulations. To test the proposed model as depicted in Figure 4 we performed molecular dynamics (MD) simulations of a monolayer of octa-ALP molecules at the vacuum-water interface. Eight molecules of **6c** were placed in an antiparallel fashion (cf. Figure 4) on top of a water layer in a rectangular simulation box with dimensions $L_a = 18.8$ Å, $L_b = 64$ Å (in accordance with the $a = 2 \times 4.7$, $b = 63.5$ Å, $\gamma = 90°$ cell deduced from the GIXD data), and an arbitrary out of plane thickness $L_c = 100$ Å sufficiently large to ensure that the octa-ALP molecules do not interact across layers, thus modeling the two-dimensional nature of the system. The simulation indicated that the octa-ALP molecules form a stable monolayer at the vacuum−water interface and that the peptide domain is organized in a β-sheet fashion with the glutamic acid residues predominantly "sticking" into the water layer and the leucine residues are directed toward the vacuum. Interestingly, the simulation shows that even in this uncompressed state, the β-sheet peptides do not lie flat on the water layer and are partially submerged in the water layer as can also be seen from the overlap between the peptide and water density profiles (cf. Supporting Information, Figure S20). The hydrophobic tails are "bundled" on top of the peptide domain and do not show any

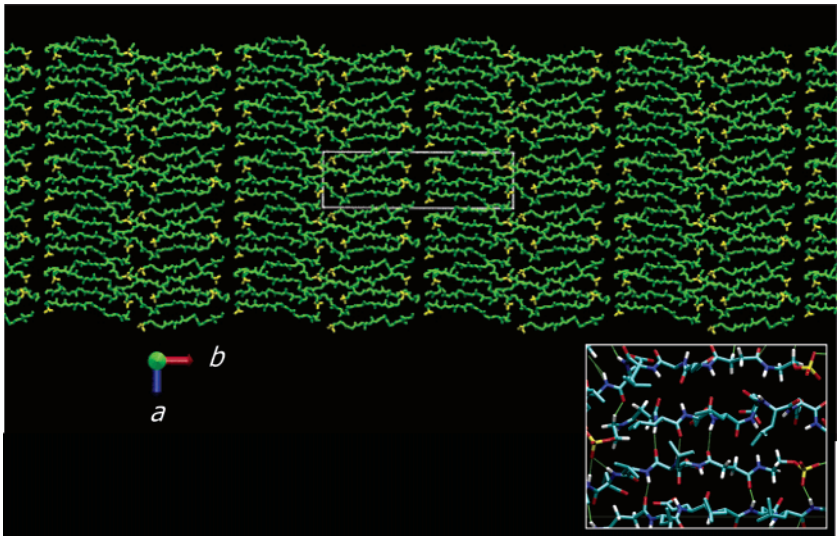

Figure 6. Snapshot of the simulation box along the *c* dimension where the original simulation box, indicated in white, is copied twice in the *-x*, *x*, *-y*, and *y* direction (orthographic top view). The green tubes indicate the peptide and succinyl part of the octa-ALP molecules and the phosphate groups are shown in yellow. The lipidic tails are omitted for clarity. Inset on the bottom right shows approximately half of the simulation box. Hydrogen atoms of the side chain are omitted for clarity, and the green dotted lines indicate hydrogen bonds.

ordering, although they have a tendency to "curl" on top of the peptide backbone, an indication of a favorable interaction with the leucine residues (cf. inset at the top right of Figure S21, Supporting Information). Sodium atoms are located predominantly in close proximity to the charged phosphate groups. The top view of the simulation box in the *c* dimension (Figure 6) shows that the octa-ALP molecules adopt an organization in the *b* dimension by forming blocks each consisting of two molecules. In the *a* dimension the peptide backbones are largely aligned which is caused by interstrand backbone-to-backbone hydrogen-bonding interactions and the formation of hydrogen bonds between phosphate groups and amide groups in the backbone (cf. inset of Figure 6). No intermolecular hydrogen bonds were formed between the double ALP width ribbons along the *b* direction. Instead, there are repulsive forces between the charged and solvated phosphates at the rim of the ribbon which lead to the interribbon gap. This result is in accordance with the model suggested based on the GIXD data in which the interactions at the center of the ribbon cannot be obtained at the rim of the ribbon. The presence of the water layer was crucial for the generation of the ordered structure. Indeed, without the water layer the organization into well-defined domains of molecules was lost. By taking the minimum *c*-value of the peptide distribution and the maximum *c*-value of the lipidic-tails distribution at half-maximum, we estimate a thickness of the monolayer of ~19 Å in reasonable agreement with the experimental value of 17 Å obtained from the GIXD experiments.

Summary and Discussion

This study presents the solid-phase synthesis of lipid conjugated β-sheet forming oligopeptides and their structural characterization as monolayers at the air−water interface. Hexa- and octa-ALP assemble into well-ordered two-dimensional monolayers as proven by the GIXD data. The monolayer architecture consists of antiparallel β-sheet ribbons induced by the peptide part, while the conjugated lipid part is folded on top of the peptide layer. The experimental observations have been rationalized by considering the "hybrid" characteristics of the system. As envisaged in the design stage, the peptide length indeed dramatically affected the behavior of the lipopeptides, especially along the film compression. The peptide part of tetra-ALP probably sinks into the subphase on increase of the surface pressure. There was no appreciable change in the β-sheet structure of hexa-ALP which remained unaltered upon compression, as indicated by the GIXD diffraction pattern, suggesting that only the nonordered part of the film, which is not detected by GIXD, yields to the applied surface pressure. The octa-ALP reacted differently to the increase in applied pressure: by a decrease in the spacing along the β-strand long axes and by a pronounced difference in Bragg rod shape along the compression. In addition, the octa-ALP exhibited a reduction of ~38% in length, from 63.5 to 39.2 Å, whereas the corresponding change in hexa-ALP was only 13%, from 52.0 to 45.6 Å (Table 2). By comparison the octa-ALP appears to be more deformable than hexa-ALP. It is possible that the eight residue β-sheet in octa-ALP has a higher tendency, relative to hexa-ALP, to bend or distort under compression. It is known that β-sheet strands have a natural tendency to twist,[22] which is also supported by our MD simulations. Therefore the longer the peptide aligned at the air−water interface, the higher the structural frustration in its backbone. The Bragg rod pattern of octa-ALP at $\pi =$ 30.1 mN/m indicates the collapse of the film into an ordered multilayer structure. The octa-ALP is the first system comprising β-sheet assemblies, which exhibits an apparent ordered multilayer structure that probably could be obtained thanks to the stabilizing contribution of the lipid tails. The compressibility of hexa-ALP was estimated, on the basis of only two experimental points, to be ~13.8 m/N. A more reliable value based on four experimental points was evaluated for octa-ALP, 12 m/N (Table 2 and Supporting Information). Both the hexa- and the octa-ALP exhibited minor changes in the (2,0) spacing, from 4.81 to 4.75 Å, with increase in surface pressure. Noteworthy, a Bragg reflection corresponding to the β-sheet hydrogen bond direction, could arise from assemblies that are ordered only in

(22) (a) Chothia, C. *J. Mol. Biol.* **1973**, *75*, 295−302. (b) Chou, K. C.; Pottle, M.; Nemethy, G.; Ueda, Y.; Scheraga, H. A. *J. Mol. Biol.* **1982**, *162*, 89−112.

the *a* direction and not along the *b* direction. Therefore, the measured intensities of the (0,1) and (2,0) reflections could be uncoupled such that the (0,1) is obtained from 2-D ordered assemblies and the β-sheet interstrand spacing (2,0) from both 1-D and 2-D ordered assemblies.

This work demonstrates that through rational design of the lipopeptide system it is possible to form complex conjugated peptide assemblies at the air−water interface. The structural flexibility, i.e., the ability of the ALP ordered assembly to adopt a variety of conformations that are dependent on changes in surface pressure was recently implicated in the formation of a new indented calcite crystal habit.[13]

Acknowledgment. S.C. is grateful to Hila Isenberg, Eran Leshem, and Silvina Federman for their invaluable help during the GIXD experiments. We thank Wim Jesse, Hans van den Elst, Nico Meeuwenoord, Fons Lefeber, and Cees Erkelens for their technical assistance. GIXD studies at beam-line BW1, Hasylab, DESY were supported by the European Community-Research Infrastructure Action under the FP6 "Structuring the European Research Area" Program (through the Integrated Infrastructure Initiative "Integrating Activity on Synchrotron and Free Electron Laser Science") and by the DanSync Program of the Danish Natural Science Research Council. K.K. thanks the Carlsberg Foundation. J.-W.H. acknowledges the Proctor & Gamble Company for a postdoctoral fellowship. The council for the Chemical Sciences of The Netherlands Organization for Scientific Research is acknowledged for a Veni Innovative Research Grant to A.K. and open competition grant to D.C.P.

Supporting Information Available: Experimental section, including additional GIXD data, CD, IR, NMR spectra, and simulation data. This material is available free of charge via the Internet at http://pubs.acs.org.

JA065479V